# TAZ inhibits acinar cell differentiation but promotes immature ductal cell proliferation in adult mouse salivary glands

Miyachi, Yosuke ; Nishio, Miki ; Otani, Junji ; Matsumoto, Shinji ; Kikuchi, Akira ; Mak, Tak Wah ; Maehama, Tomohiko ; Suzuki, Akira

(Citation)
Genes to Cells,26(9):714-726

(Issue Date)
2021-09

(Resource Type)
journal article

(Version)
Accepted Manuscript

# TAZ inhibits acinar cell differentiation but promotes immature ductal cell proliferation in adult mouse salivary glands

Yosuke Miyachi[1,6], Miki Nishio[1,6], Junji Otani[1], Shinji Matsumoto[2], Akira Kikuchi[2], Tak Wah Mak[3,4,5], Tomohiko Maehama[1,7,8] and Akira Suzuki[1,7,8]

[1]Division of Molecular and Cellular Biology, Kobe University Graduate School of Medicine, Kobe, Japan

[2]Department of Molecular Biology and Biochemistry, Graduate School of Medicine, Osaka University, Suita, Japan

[3]The Princess Margaret Cancer Centre, University Health Network, Toronto, Canada

[4]Departments of Immunology and Medical Biophysics, University of Toronto, Toronto, Canada

[5]Department of Pathology, LKS Faculty of Medicine, The University of Hong Kong, Hong Kong, SAR

[6]Equal contribution as first author.

[7]Equal contribution as last author.

[8]Corresponding authors:

Tomohiko Maehama, Division of Molecular and Cellular Biology, Kobe University Graduate School of Medicine, Kusunoki-cho 7-5-1, Chuo-ku, Kobe, Hyogo, 650-0017, Japan

Tel:+81-78-382-6052; Fax:+81-78-382-6053; E-mail: tmaehama@med.kobe-u.ac.jp

Akira Suzuki, Division of Molecular and Cellular Biology, Kobe University Graduate School of Medicine, Kusunoki-cho 7-5-1, Chuo-ku, Kobe, Hyogo, 650-0017, Japan

Tel:+81-78-382-6051; Fax:+81-78-382-6053; E-mail: suzuki@med.kobe-u.ac.jp

**Short Running title:** Role of TAZ in adult mouse salivary gland.

**Keywords:** TAZ, Hippo, MOB1, Salivary gland, Acinar cells, Ductal cells

Total characters count (excluding figure legends, references, tables and supplementary materials): 31,676

**Number of Figures:** 6

**Number of Tables:** 0

**Supporting Information:** Supplementary Table S1, Figures and Legends S1-S4

**Abstract**

There are currently no treatments for salivary gland diseases, making it vital to understand signaling mechanisms operating in acinar and ductal cells so as to develop regenerative therapies. To date, little work has focused on elucidating the signaling cascades controlling the differentiation of these cell types in adult mammals. To analyze the function of the Hippo-TAZ/YAP1 pathway in adult mouse salivary glands, we generated *ad*MOB1DKO mice in which both MOB1A and MOB1B were TAM-inducibly deleted when the animals were adults. Three weeks after TAM treatment, *ad*MOB1DKO mice exhibited smaller submandibular glands (SMGs) than controls with a decreased number of acinar cells and an increased number of immature dysplastic ductal cells. The mutants suffered from reduced saliva production accompanied by mild inflammatory cell infiltration and fibrosis in SMGs, similar to the Sjogren's syndrome. MOB1-deficient acinar cells showed normal proliferation and apoptosis but decreased differentiation, leading to an increase in acinar/ductal bi-lineage progenitor cells. These changes were TAZ-dependent but YAP1-independent. Biochemically, MOB1-deficient salivary epithelial cells showed activation of the TAZ/YAP1 and β-catenin in ductal cells, but reduced SOX2 and SOX10 expression in acinar cells. Thus, Hippo-TAZ signaling is critical for proper ductal and acinar cell differentiation and function in adult mice.

## 1. Introduction

The saliva that constantly lubricates the mammalian mouth aids in swallowing, digestion and combatting infection (Mese & Matsuo 2007). Saliva is produced by salivary glands that are made up of a branched epithelial network of ducts ending in the acini, which are responsible for synthesizing and secreting saliva. Loss of saliva is a frequent consequence of the radiation therapy used to treat head-and-neck cancer or autoimmune diseases like Sjögren's syndrome (Saleh *et al.* 2015). However, there are currently no effective means of inducing the *in vivo* regeneration of acini to increase their saliva production.

Previous work has defined many steps of early salivary gland development in the mammalian fetus. Indeed, the epithelial cells in the adult gland are all derived from fetal epithelial cells expressing Trp63 (initial placode), cytokeratin 14 (CK14), Sox2, Sox9 and Sox10 (Lombaert *et al.* 2013; Chatzeli *et al.* 2017; Song *et al.* 2018; Athwal *et al.* 2019). However, as development of the initial fetal gland proceeds, lineage restriction ensues that ensures postnatal glands contain separate lineages of ductal, myoepithelial, and acinar cells. It has been shown that acinar cells in the submandibular gland (SMG) of mature mice can self-renew during postnatal growth to maintain homeostasis (Aure *et al.* 2015b; Maruyama *et al.* 2016). These glands are also constantly replenished by bi-lineage progenitor cells that reside within the intercalated duct (ID) region that lies immediately adjacent to the acini. These progenitors can differentiate into either duct cells or acinar secretory cells (Aure *et al.* 2015a; Schwartz-Arad *et al.* 1988), but the signaling pathways that trigger these cell fate decisions are not yet well understood. Thus, defining these mechanisms could pave the way for novel therapies designed to regenerate damaged salivary glands. In particular, a focus on determining the postnatal signals that control the development and functions of the salivary ducts and acini would be helpful to advance the field.

Our group has been studying the mammalian Hippo signaling pathway in various mouse tissues using engineered mutants (Nishio *et al.* 2017; Maehama *et al.* 2020). Hippo signaling generally terminates in the phosphorylation and negative regulation of the transcriptional co-activators "transcriptional co-activator with PDZ-binding motif" (TAZ) (also known as WW domain containing transcriptional regulator 1; WWTR1) and its paralogue "Yes-associated protein-1" (YAP1). Unphosphorylated TAZ and YAP1

interact mainly with nuclear TEA domain transcription factors (TEADs) that activate the expression of target genes involved in controlling cell growth and self-renewal, inflammatory cell migration, and fibrosis (Nakatani *et al.* 2017; Murakami *et al.* 2017; Wang *et al.* 2016). Many external entities can regulate the Hippo-TAZ/YAP1 pathway and thus TAZ/YAP1 activities, including signaling by certain integrins, growth factors, hormones, and G-protein-coupled receptors, as well as the degree of cell density or rigidity of the extracellular matrix (ECM), or activities of components of adherens junction complexes (Nakatani *et al.* 2017). These triggers impinge on the core of the Hippo pathway, which is made up of the large tumor suppressor homolog (LATS) kinases and the mammalian STE20-like protein (MST) kinases. LATS and MST kinase activities are greatly enhanced when they bind to their respective adaptor proteins "mps one binder kinase activator-1" (MOB1A/1B) and "salvador homolog-1" (SAV1) (Nakatani *et al.* 2017). When TAZ/YAP1 bind to components of the adherens or tight junctions (Chan *et al.* 2011; Schlegelmilch *et al.* 2011; Wang *et al.* 2012; Skouloudaki *et al.* 2009), they are phosphorylated by LATS and thereby confined to the cytoplasm. The E3-ubiquitin ligase $SCF\beta^{TRCP}$ then ubiquitinates the phosphorylated TAZ/YAP1 molecules and promotes their proteasome-mediated degradation, blocking TEAD-mediated gene transcription.

Previous work has demonstrated that TAZ/YAP1 is critical for the formation of many organs involving branched structures, including the mammary gland, pancreas, lung and kidney (Chen *et al.* 2014; Gao *et al.* 2013; George *et al.* 2012; Mahoney *et al.* 2014; Reginensi *et al.* 2013). TAZ/YAP1 activity is required to expand progenitor cell populations in multiple tissues, whereas conditional *Taz/Yap1* deletion in organ-specific stem cells either inhibits stem cell specification or induces premature differentiation (Mahoney *et al.* 2014; Panciera *et al.* 2016; Zhao *et al.* 2014). However, the function of TAZ/YAP1 in salivary gland biology is somewhat controversial. Several lines of evidence suggest that Hippo signaling and TAZ/YAP1 regulation are important drivers of salivary gland development and function: (1) In explant cultures of mouse SMGs at E13.5, siRNA-mediated suppression of LATS2 produces a branching defect (Enger *et al.* 2013); (2) *Lats1/2* deletion in mouse embryonic salivary epithelial cells results in a marked decrease in branching and an uncontrolled increase in the ductal domain driven by proliferating $CK5^{+}CK14^{+}$ ductal precursor cells (Szymaniak *et al.* 2017); and (3) YAP1 deficiency in epithelial cells of embryonic SMGs is associated with a decrease in

epiregulin expression that inhibits the proliferation of $CK5^{+}CK14^{+}$ ductal precursor cells, resulting in a loss of ductal structures (Szymaniak *et al.* 2017). These findings imply that proper Hippo signaling is required during SMG-branching morphogenesis to generate mature secondary ducts. On the other hand, Hwang *et al.* have reported that TAZ/YAP1 siRNA decreases immortalized salivary epithelial cell apoptosis induced by TNF-α and Lysophosphatidic acid (LPA), suggesting that TAZ/YAP1 normally act to promote the LPA-induced death of salivary epithelial cells (Hwang *et al.* 2014). To date, there have been no reports on the functions of the Hippo-TAZ/YAP1 pathway in adult mouse salivary gland homeostasis, and no investigation of whether there are differences in the roles of TAZ vs. YAP1 in this tissue. Here we present the results of our study using a genetic approach to examine the role of Hippo-TAZ/YAP1 signaling in maintaining salivary gland homeostasis in adult mice, and show our mutant mice become the model of Sjogren's syndrome in human.

## 2. Results

### 2.1 Loss of *Mob1a/1b* reduces acinar cells and increases immature ductal cells with dysplasia

To examine the roles of TAZ/YAP1 in mature mouse salivary gland, we generated adult mutant mice with postnatal deletion of MOB1A and MOB1B (*ad*MOB1DKO). To this end, we crossed *Mob1a*$^{flox/flox}$*;Mob1b*$^{-/-}$ mice (Nishio *et al.* 2012) to *Rosa26-CreERT2*-Tg mice (Ventura *et al.* 2007) to produce *Rosa26-CreERT2;Mob1a*$^{flox/flox}$*;Mob1b*$^{-/-}$ progeny in which *Mob1a/1b* deletion could be post-natally induced by treatment with tamoxifen (TAM). We then i.p.-administered TAM for 5 days to *Rosa26-CreERT2;Mob1a*$^{flox/flox}$*;Mob1b*$^{-/-}$ mice as well as to control *Mob1a*$^{flox/flox}$*;Mob1b*$^{-/-}$ mice and *Rosa26-CreERT2;Mob1a*$^{flox/flox}$*;Mob1b*$^{+/+}$ mice when the animals were all 35-42 days old. We sacrificed these mice at 7, 10, 14 or 21 days after TAM initiation (post-TAM) and analyzed their SMGs (Figure S1a). None of the TAM-treated *Rosa26-CreERT2;Mob1a*$^{flox/flox}$*;Mob1b*$^{-/-}$ mice (*ad*MOB1DKO) survived past 3-5 weeks post-TAM, possibly because of impaired food intake and/or body fluid loss due to skin damage. Therefore, we collected SMGs at various timepoints during an observation period of up to 3 weeks post-TAM. Because there were no histological differences among (1) *Mob1a*$^{flox/flox}$*;Mob1b*$^{-/-}$ without TAM, (2) *Mob1a*$^{flox/flox}$*;Mob1b*$^{-/-}$ with TAM, and (3) *Rosa26-CreERT2;Mob1a*$^{flox/flox}$*;Mob1b*$^{+/+}$ with TAM mice (Figure S1b), we selected *Mob1a*$^{flox/flox}$*;Mob1b*$^{-/-}$ with TAM mice as representative controls. Crossing of *ad*MOB1DKO mice with *Rosa26-LSL-tdTomato* reporter mice (Madisen *et al.* 2010) confirmed that most ductal cells and acinar cells had undergone *Mob1a/1b* deletion, as determined by RFP positivity (Figure S2).

We next examined the SMGs of *ad*MOB1DKO mice in more detail. By day 14 post-TAM and beyond, *ad*MOB1DKO mice displayed smaller salivary glands (Figure 1a, left). The total weight and cell number of SMGs of these mutants at 3 weeks post-TAM were 32% lower than those in controls (Figure 1a, right). Notably, the total number of aquaporin 5-expressing (AQP5)$^+$ acinar cells was 63% lower than that in control mice. On the other hand, although the total cell number of CK7$^+$ ductal cells was normal in *ad*MOB1DKO mice (Figure 1b), the number of CK14$^+$CK7$^+$ immature ductal cells was increased 2.7 times, and CK14$^-$CK7$^+$ mature ductal cells were decreased by 23% in mutant SMGs (Figure 1c). Histologically, some ductal cells in the mutant underwent focal

hyper-proliferation and generated a lump without obvious lumen structure (Figure 1b), while other ductal cells exhibited dysplasia and enlarged nuclei (Figure 1d). Salivary gland cancers were not detected during the relatively short observation period. Thus, *ad*MOB1DKO salivary glands exhibit 'acinar cell hypoplasia and immature ductal cell hyperplasia with dysplasia.

**2.2 Decreased saliva production, increased inflammatory cells and fibrosis similar to Sjögren's syndrome in *ad*MOB1DKO mice**

Because the total number of acinar cells was decreased in *ad*MOB1DKO mice, we analyzed their saliva production. We compared amounts of saliva secreted by control and *ad*MOB1DKO mice at 3 weeks post-TAM and found that the mutants produced 44% less saliva than controls of the same age (Figure 2a). In addition, histological examination of the SMGs of these *ad*MOB1DKO mice revealed modest levels of inflammatory cell infiltration (CD45 positive) and fibrosis (Sirius Red stain) (Figure 2b). All of these phenotypic features are reminiscent of aspects of Sjögren's syndrome in humans.

**2.3 Acinar cells lacking MOB1 exhibit normal proliferation and apoptosis, but MOB1-deficient ductal cells show increased turnover**

To determine why acinar cells were decreased in *ad*MOB1DKO SMGs, we analyzed the percentages of $PCNA^+$ (proliferation marker) and $TUNEL^+$ (apoptosis marker) cells among $AQP5^+$ acinar cells in control and mutant SMGs. We found no significant differences in percentages of either $PCNA^+$ cells (Figure 3a) or $TUNEL^+$ cells (Figure 3b), indicating that the deficit in acinar cells in mutant SMG was not due to either decreased cell proliferation nor increased cell death. In contrast, the proliferation and apoptosis of $CK7^+$ ductal cells were increased 18 and 9 times, respectively, in mutant SMG (Figure 3a, 3b), indicating rapid turnover. Considering the lack of obvious cell death among acinar cells of *ad*MOB1DKO mice, we concluded that the observed decrease in acinar cells was not a deadly consequence of lymphocyte infiltration into the SMG.

**2.4 Decreased differentiation toward acinar cells, but increased numbers of acinar/ductal bi-lineage progenitors, in the absence of MOB1**

To more closely examine acinar cell differentiation, we took advantage of a TAM-inducible murine *Mob1a/1b* DKO salivary epithelial cell clone (*im*MOB1DKO) that arose by spontaneous immortalization of salivary gland cells from *Rosa26-CreERT2;Mob1a*$^{flox/flox}$*;Mob1b*$^{-/-}$ mice cultured without TAM. When cultured in Matrigel without TAM, these cloned MOB1-expressing *im*MOB1DKO cells increased their mRNA expression levels of the acinar cell markers *Aqp5* and amylase1 (*Amy1a*), and decreased those of the ductal markers *Krt19* and *Krt7* (Figure 4a). This observation is consistent with previous report that a human salivary gland epithelial cell line can be differentiated into acinar cells on Matrigel (Royce *et al.* 1993). In contrast, when these *im*MOB1DKO cells were cultured with TAM for 14 days, they showed decreased mRNA levels of *Amy1a* and *Aqp5* but increased mRNA levels of *Krt19* and *Krt7* (Figure 4b). Immunostaining experiments confirmed that cells positive for both AQP5 and CK14 (immature ductal cell marker) among the ductal-shaped cells were increased more in SMGs of *ad*MOB1DKO mice than those of control mice (Figure 4c). These data suggest that the bi-lineage progenitor resident in adult SMG is influenced by MOB1 function.

### 2.5 Activation of TAZ rather than YAP1 can explain the phenotype of *ad*MOB1DKO mice

We next investigated the biochemical effects of *Mob1a/1b* loss on Hippo components using cells isolated from SMGs of *ad*MOB1DKO mice at 3 weeks post-TAM. As expected, *ad*MOB1DKO cells showed strong increases in both total TAZ and total YAP1 proteins as determined by immunoblotting (Figure 5a). Immunohistochemical analysis of SMGs from control and *ad*MOB1DKO mice revealed that, in control SMG, both TAZ and YAP1 were faintly detected in the cytoplasm of acinar and ductal cells (Figure 5b, left). In contrast, in *ad*MOB1DKO SMG, the expression levels of both TAZ and YAP1 in the nucleus were substantially increased in ductal and acinar cells (Figure 5b, right).

To determine whether *Mob1a/1b*-deficient salivary phenotypes depended mainly on TAZ or on YAP1, we generated two strains of triple knockout (TKO) mice: MOB1A/1B&TAZ TKO [*Mob1a/1b* plus *Taz* (*Rosa26-CreERT2;Mob1a*$^{flox/flox}$*;Mob1b*$^{-/-}$*;Taz*$^{flox/flox}$;+TAM]; and MOB1A/1B&YAP1 TKO [*Mob1a/1b* plus *Yap1* (*Rosa26-CreERT2;Mob1a*$^{flox/flox}$*;Mob1b*$^{-/-}$*;Yap1*$^{flox/flox}$;+TAM]. Efficient YAP1 or TAZ loss in most cells in the SMGs of these YAP1 TKO and TAZ

TKO mice was confirmed by immunoblotting (Figure S3). H&E staining of SMG sections from these mutants plus SMGs from *Mob1a/1b* DKO (*Rosa26-CreERT2; Mob1a*$^{flox/flox}$*;Mob1b*$^{-/-}$;+TAM), and control (*Mob1a*$^{flox/flox}$*;Mob1b*$^{-/-}$*;Taz*$^{flox/flox}$;+TAM) mice revealed a striking difference between TAZ and YAP1. The decrease in acinar cells and the increase in immature ductal cells observed in *ad*MOB1DKO adult mice were dramatically suppressed by additional *TAZ* loss, but were not significantly affected by additional YAP1 loss (Figure 5c). Thus, the salivary phenotypes of *ad*MOB1DKO adult mice depend primarily on TAZ rather than YAP1.

### 2.6 Inactivation of SOXs but activation of the β-catenin in *ad*MOB1DKO SMG

Acinar cell formation is regulated by SOX2 and SOX10 (Emmerson *et al.* 2017), (Athwal *et al.* 2019). We therefore analyzed the expression of these genes in *ad*MOB1DKO SMG at 3 weeks post-TAM. Immunoblotting revealed that, in control SMG, SOX2 was expressed in a certain population of acinar and ductal cells, whereas SOX10 was expressed mainly in acinar cells (Figure 6a, left). On the other hand, protein expression levels of both SOX2 and SOX10 in the nucleus were significantly reduced in the SMG of *ad*MOB1DKO mice at 3 weeks post-TAM compared to controls (Figure 6a, right).

In the SMG of mutant mice with constitutive activation of either the WNT or Hedgehog (Hh) pathway, immature ductal cells are increased and acinar cells are decreased (Hai *et al.* 2010). We therefore examined the activation of β-catenin (WNT signaling target) or GLI2 (Hh signaling target), as the downstream molecules of TAZ/YAP1 activation, in *ad*MOB1DKO SMGs using antibodies recognizing activated β-catenin or GLI2 (van Noort *et al.* 2002; Sugiyama *et al.* 2016). We found that β-catenin was significantly activated in MOB1-deficient SMG, particularly in the immature ductal cells (Figure 6b), whereas GLI2 was not altered by the MOB1 deficiency (Figure S4). Thus, the TAZ-SOX and TAZ-β-catenin signaling may be important for the phenotypes observed in mice lacking the Hippo core component MOB1 in the salivary gland.

## *3. Discussion*

To date, studies of mutant mice experiencing inhibition or loss of LATS kinase function beginning at the embryonic stage have revealed expansion of $CK5^+CK14^+$ salivary ductal precursor cells, a severe lack of ductal branching, and an accumulation of inflammatory cells similar to that observed in human Sjögren's syndrome (SS) (Enger *et al.* 2013; Szymaniak *et al.* 2017). In our study, we have demonstrated for the first time that postnatal activation of TAZ (rather than YAP1) decreases acinar cells in adult mice *in vivo*. We have also provided evidence pointing to a possible mechanism for this observation. We hypothesize that the decrease in acinar cells in *ad*MOB1DKO SMG may be due to impaired acinar differentiation of bi-lineage progenitor cells and/or the transdifferentiation of acinar cells into the ductal lineage. We base this theory on the following: (1) the decreased number of acinar cells in *ad*MOB1DKO SMG; (2) the reduced levels of acinar lineage mRNAs in MOB1-deficient immortalized clonal salivary epithelial cells; and (3) the increased number of acinar/ductal bi-lineage cells in *ad*MOB1DKO SMG. In addition, MOB1-deficient adult salivary glands showed reduced saliva production as well as moderately increased inflammatory cell infiltration and fibrosis. These features are similar to those of human SS.

SS is generally considered to be an acquired autoimmune disease of the salivary and lacrimal glands (Jonsson *et al.* 2007). The principal manifestations of SS include hyposalivation and ocular dryness. This loss of secretory functions in SS is largely believed to result from cytotoxicity caused by progressive lymphocytic infiltration in the salivary and lacrimal glands (Price & Venables 1995). Considering that the inflammatory cell infiltration and fibrosis in our mutant SMG were mild, and no increase in apoptosis was observed in the mutant acinar cells, the phenotypes of *ad*MOB1DKO SMG are not likely to be the consequences of an autoimmune disease. However, to date, the etiology of SS remains controversial, and increasing evidence implicates glandular structural defects as primary contributors to at least some SS cases (Hatzopoulos *et al.* 2002; Boki *et al.* 2001). Key findings supporting this contention come from studies of the NOD strain of mutant mice, which have been used extensively as a model of SS or type 1 diabetes (Soyfoo *et al.* 2007; Kodama *et al.* 2003; Lonyai *et al.* 2008). The salivary glands of NOD mice exhibit structural defects and hyposalivation that are independent of lymphocytic

infiltration (Lonyai *et al.* 2008; Price & Venables 1995). Similarly, the degrees of acinar cell atrophy and salivary gland hypofunction in SS patients do not always correspond to the observed level of lymphocytic infiltration (Jonsson *et al.* 2007; Ewert *et al.* 2010; Velozo *et al.* 2009; Barrera *et al.* 2012; Delaleu *et al.* 2008). Thus, rather than the immune system, structural defects may in fact be the primary culprit causing the salivary gland dysfunction in human SS. Interestingly, salivary acinar cells of human SS patients display mis-localization of TAZ in the nucleus (Enger *et al.* 2013). For these reasons, our *ad*MOB1DKO mice may represent a useful model of SS.

The phenotypes of our *ad*MOB1DKO mutants are also similar to those of wild type mice that have undergone salivary duct ligation (Figure S5a). Such ligation can serve as a model of the duct obstruction caused by tumors or salivary stones (Hai *et al.* 2010). Indeed, we observed a shrinking of the ductal lumen in the lumps of hyperplastic ductal cells seen in some *ad*MOB1DKO SMGs (Figure 1b). However, because saliva never accumulated in these mutant glands, and our TAM-inducible Mob1-deficient immortalized salivary epithelial cell line showed decreased expression of acinar lineage mRNAs, the phenotypes of *ad*MOB1DKO mice cannot be explained simply by duct stenosis. Intriguingly, TAZ expression is markedly increased in acinar cells following salivary duct ligation (Figure S5b, S5c), indicating that an increase in TAZ may account for not only the phenotypes of mice with loss of MOB1 but also those experiencing duct ligation.

YAP1 deficiency in mice at the embryonic stage results in loss of the early salivary gland ductal progenitor population and ductal structures (Szymaniak *et al.* 2017). However, these deficits are not observed in TAZ-deficient mice, establishing that it is YAP1 that is important for salivary gland morphogenesis in the embryo. However, the phenotype of our *ad*MOB1DKO adult mice, where loss of MOB1 was post-natal, depends on TAZ rather than on YAP1 (Figure 5c). According to an RNA sequencing analysis of wild type murine salivary glands (https://sgmap.nidcr.nih.gov/sgmap/sgexp.html), *Taz* transcripts are 4 times higher than *Yap1* transcripts in adult mouse SMG, whereas *Yap1* transcripts in $Kit^{+}CK5^{+}$ precursor sublingual ductal cells in mouse embryos (E15) are 5 times higher than *Taz* transcripts. This stage-specific oscillation between *Yap1* and *Taz* transcriptional dominance may underpin the phenotypes of our mutant SMGs.

*Sox2* and *Sox10* are direct downstream transcriptional targets of the TAZ/YAP1-TEAD complex, and both are normally expressed in cells that give rise to salivary ducts and acini (Aure *et al.* 2019; Li *et al.* 2019). However, genetic ablation of *Sox2* in salivary epithelium impaired the generation of acini but not ducts (Emmerson *et al.* 2017). It was further shown that Sox2 is essential both for facilitating Sox10 expression and targeting acinar-specific genes (Emmerson *et al.* 2017). Genetic deletion of *Sox10* in salivary epithelium resulted in a loss of acinar secretory units but retention of the ductal tree (Athwal *et al.* 2019). Overexpression of *Sox10* in ductal progenitors enhanced their plasticity and induced their differentiation into secretory units (Athwal *et al.* 2019). Thus, following its activation by Sox2, Sox10 acts as a master regulator of secretory unit differentiation in salivary glands. Although it has been determined that, in wild type mice, TAZ and YAP1 usually increase the expression of these SOXs, they can also decrease their expression in a cell context-dependent manner (Goto *et al.* 2018). We observed that SOX2 and SOX10 were significantly decreased in our mutant SMGs. Thus, impaired SOX2 and SOX10 expression downstream of TAZ may explain the SMG phenotypes of our adult MOB1-deficient mice.

Another factor may be the mutual crosstalk between the TAZ/YAP1 and WNT, TAZ/YAP1 and Hh, WNT/Hh and SOX2/SOX10, and SOX2 and SOX10 signaling cascades, all of which are reported to control each other's activity (Nishio *et al.* 2015; Uka *et al.* 2020; Yin *et al.* 2017; Ye *et al.* 2014; Lee *et al.* 2016; Castillo-Azofeifa *et al.* 2018; Huang *et al.* 2018). WNT signaling is usually active within the intercalated duct region in postnatal glands (Hai *et al.* 2010). Specific post-natal inhibition of WNT signaling in the $K5^+$ cell lineage significantly impairs the maturation of granular convoluted tubules, whereas forced activation of the WNT and Hh pathways promotes the expansion of salivary gland stem/progenitor cells and ductal cells but the loss of acinar cells (Hai *et al.* 2010). These phenotypes are remarkably similar to those of our *ad*MOB1DKO mutants. We did indeed observe activation of the β-catenin in our mutant SMGs, reinforcing our hypothesis that altered TAZ activation/regulation due to loss of MOB1, and the effects of this alteration on the WNT and SOXs pathways, may explain the salivary gland phenotypes of our adult *ad*MOB1DKO mice.

Our study has clarified the function of TAZ in the adult mouse salivary gland and established that the Hippo-TAZ pathway is important for proper ductal and acinar cell

development in these structures. The knowledge gained from our work may be instructive for designing therapies to prevent or reduce the effects of salivary gland damage caused by irradiation, autoimmune responses, or chemical agents. Furthermore, our mutant mice may serve as a helpful model with which to explore future putative regenerative strategies to treat damaged salivary glands in patients.

## *4. Experimental Procedures*

### *Mice*

Mouse strains used in this study were: *Mob1a*$^{flox/flox}$*;Mob1b*$^{-/-}$ (Nishio *et al.* 2012); *Rosa26-CreERT2-Tg* (The Jackson Laboratory); *Rosa26-CreERT2-Tg*;*Rosa26-LSL-tdTomato* reporter (The Jackson Laboratory); and *Taz*$^{flox/flox}$ (kindly provided by Dr. J. Wrana). *Yap1*$^{flox/flox}$ mice were generated using *Yap1*$^{flox/flox}$ ES cells from the Knockout Mouse Project Repository. Adult *Mob1a/1b* double homozygous mutant mice (*Rosa26-CreERT2;Mob1a*$^{flox/flox}$*;Mob1b*$^{-/-}$ mice; designated *ad*Mob1DKO) were generated by mating *Rosa26-CreERT2*-Tg mice to *Mob1a*$^{flox/flox}$*;Mob1b*$^{-/-}$mice. *Mob1a*$^{flox/flox}$*;Mob1b*$^{-/-}$ mice *and Rosa26-CreERT2;Mob1a*$^{flox/flox}$*;Mob1b*$^{+/+}$ mice, which were generated by mating *Rosa26-CreERT2*-Tg mice to *Mob1a*$^{flox/flox}$*;Mob1b*$^{+/+}$mice, were used as controls. Postnatal *Mob1* deletion was induced by administering tamoxifen (TAM; Toronto Research Chemicals, Toronto, Canada) 1 mg/day (i.p.) for 5 days starting on P35–39. *Mob1a/1b* plus *Taz* TKO (*Rosa26-CreERT2;Mob1a*$^{flox/flox}$*;Mob1b*$^{-/-}$*;Taz*$^{flox/flox}$) and *Mob1a/1b* plus *Yap1* TKO (*Rosa26-CreERT2;Mob1a*$^{flox/flox}$*;Mob1b*$^{-/-}$*;Yap1*$^{flox/flox}$) triple mutant mice were generated by mating ad*Mob1*DKO mice with *Yap1*$^{flox/flox}$ or *Taz*$^{flox/flox}$ mice, respectively. *Mob1a*$^{flox/flox}$*;Mob1b*$^{-/-}$*;Taz*$^{flox/flox}$ mice (control mice in Supplementary Figure 3) were generated by mating *Mob1a*$^{flox/flox}$*;Mob1b*$^{-/-}$ mice to *Taz*$^{flox/flox}$ mice. Primers used for genotyping PCR are listed in Supplementary Table S1.

### *Saliva collection*

Animals were placed in a restraining device and stimulated with Pilocarpine (10 mg/Kg, Fujifilm Wako Chemicals), and saliva was collected for 60 min. Saliva volume was determined gravimetrically, assuming that saliva has a density of 1 g/ml.

### *Isolation of TAM-inducible or non-inducible primary Mob1 DKO salivary gland cells (imMob1DKO cells)*

A previously described salivary gland isolation protocol (Hisatomi *et al.* 2004) was used to obtain TAM-inducible primary salivary gland cells (*im*Mob1DKO cells) from 3-week-old *Rosa26-CreERT2;Mob1a*$^{flox/flox}$*;Mob1b*$^{-/-}$ mice without TAM. Briefly, mouse

submandibular glands (SMGs) were excised, minced, and digested by collagenase and hyaluronidase, followed by further digestion with dispase. Resultant primary salivary gland cells were cultured in DMEM/F12 medium supplemented with 2 mM glutamine, 20 ng/ml EGF (PeproTech), 20 ng/ml FGF2 (PeproTech), 1× Insulin-Transferrin-Selenium (Gibco), and 1 μM dexamethasone. Spontaneously immortalized *im*Mob1DKO cells were generated by continuous culture for more than 15 passages. Loss of *Mob1a/1b* in these cells *in vitro* was induced by treating them with TAM (0.5 μM; Toronto Research Chemicals) for 2 days.

***Immunoblotting***

Cells were homogenized in Lysis Buffer (10mM Tris-HCl pH7.4, 200mM NaCl, 1mM EDTA) containing a protein inhibitor cocktail (Nacalai Tesque) and subjected to immunoblotting using a standard protocol. Primary antibodies recognizing the following proteins were used: MOB1A/1B (Cell Signaling); YAP1 (Cell Signaling); TAZ (Cell Signaling); Actin (Sigma). Primary Abs were detected using HRP-conjugated secondary Abs (Cell Signaling).

***Tissue immunostaining***

Mouse tissues were either fixed in 4% paraformaldehyde in PBS and embedded in paraffin, or snap-frozen in optimal cutting temperature (OCT) compound, and sectioned (5 μm). Antigen retrieval was conducted by the incubation for 10 min at 121°C in 10 mM citrate buffer (pH 6). For immunohistochemistry (IHC), fixed sections were incubated overnight at 4°C with primary Abs recognizing: Ki-67 (Abcam); AQP5 (Alomone Labs); CK7 (Abcam); CK14 (Invitrogen); CD45 (Biolegend); PCNA (BD); YAP1 (Sigma-Aldrich); TAZ (Cell Signalling Technology); RFP (Fujifilm Wako Chemicals); active β-catenin (Millipore); GLI2 (Abcam); SOX2 (Proteintech); or SOX10 (Proteintech). HRP- and AP-conjugated anti-rabbit/mouse IgG antibodies (DAKO) were used for DAB and New Fuchsin staining, respectively. Alexa 488- and Alexa 594-conjugated anti-rabbit/mouse IgG antibodies (Invitrogen) were used for immunofluorescent staining. TUNEL staining was performed using a kit in accordance with the manufacturer's instructions (Roche). For quantitative analyses, positively-stained cells were counted and normalized against the total cell number (at least 1,000 cells/sample). The total cell

number of each sample was determined by counting DAPI- or hematoxylin-positive cells.

***Quantitative reverse transcription PCR (qRT-PCR)***

Total RNA was isolated from cells using RNAiso Plus (Takara) according to the manufacturer's instructions. Real-time qRT-PCR analysis was carried out with THUNDERBIRD SYBR qPCR Mix (Toyobo) following the manufacturer's instructions and using the primers listed in Supplementary Table S1. PCR amplifications were performed using the StepOne real-time PCR system (Applied Biosystems). Ct values for each gene amplification were normalized by subtracting the Ct value calculated for *Gapdh*. These normalized gene expression values were deemed to represent the relative quantity of mRNA in a sample.

***Duct ligation***

Female Balb/c mice (5 weeks old) were anesthetized and held in the supine position with the neck extended. An incision was made in the midline of the neck and both SMGs were exposed. After ligation of the main excretory duct, the neck was sutured as described previously (Hisatomi *et al.* 2004). After 7 days, SMG samples were collected and subjected to tissue immunostaining as described above.

***Statistics***

Unless otherwise indicated, all results are expressed as the mean ± SEM. Statistical comparisons between different groups were performed using the 2-tailed Student's t test. For all statistical analyses, differences of $P<0.05$ were considered statistically significant. For all Figures, $*P<0.05$, $**P<0.01$, $***P<0.001$. All experiments were repeated at least 3 times with at least 3 cultures or mice per group.

**Acknowledgements**

We are grateful to Dr. S. Fujii (Osaka University) for their technical assistance. We also thank Dr. J. Wrana (Lunenfeld-Tanenbaum Research Institute) for *Taz*$^{flox/flox}$ mice. We appreciate the generous funding provided by the Japanese Society for the Promotion of Science (JSPS; grants17H01400,26114005,26640081); the Cooperative Research Project Program of the MIB, Kyushu University; Nanken-Kyoten, Tokyo Medical and Dental University (TMDU); the Japanese Agency for Medical Research and Development [P-CREATE(AMED) grant; JP19cm0106114]; and the Kanzawa Medical Research Foundation.

**Supporting Information**

Supporting Information containing Table S1, Figure S1-S4 and their legends is available on line.

**Disclosure Statement**

The authors have no conflicts of interest to declare.

**Orcid**

Tomohiko Maehama: https://orcid.org/0000-0002-9685-2317

Akira Suzuki: https://orcid.org/0000-0002-5950-8808

***References***


Athwal, H.K., Murphy, G., 3rd, Tibbs, E., Cornett, A., Hill, E., Yeoh, K., Berenstein, E., Hoffman, M.P. & Lombaert, I.M.A. (2019) Sox10 Regulates Plasticity of Epithelial Progenitors toward Secretory Units of Exocrine Glands. *Stem Cell Reports* **12**, 366-380.

Aure, M.H., Arany, S. & Ovitt, C.E. (2015a) Salivary Glands: Stem Cells, Self-duplication, or Both? *J Dent Res* **94**, 1502-1507.

Aure, M.H., Konieczny, S.F. & Ovitt, C.E. (2015b) Salivary gland homeostasis is maintained through acinar cell self-duplication. *Dev Cell* **33**, 231-237.

Aure, M.H., Symonds, J.M., Mays, J.W. & Hoffman, M.P. (2019) Epithelial Cell Lineage and Signaling in Murine Salivary Glands. *J Dent Res* **98**, 1186-1194.

Barrera, M.J., Sanchez, M., Aguilera, S., Alliende, C., Bahamondes, V., Molina, C., Quest, A.F., Urzua, U., Castro, I., Gonzalez, S., Sung, H.H., Albornoz, A., Hermoso, M., Leyton, C. & Gonzalez, M.J. (2012) Aberrant localization of fusion receptors involved in regulated exocytosis in salivary glands of Sjogren's syndrome patients is linked to ectopic mucin secretion. *J Autoimmun* **39**, 83-92.

Boki, K.A., Ioannidis, J.P., Segas, J.V., Maragkoudakis, P.V., Petrou, D., Adamopoulos, G.K. & Moutsopoulos, H.M. (2001) How significant is sensorineural hearing loss in primary Sjogren's syndrome? An individually matched case-control study. *J Rheumatol* **28**, 798-801.

Castillo-Azofeifa, D., Seidel, K., Gross, L., Golden, E.J., Jacquez, B., Klein, O.D. & Barlow, L.A. (2018) SOX2 regulation by hedgehog signaling controls adult lingual epithelium homeostasis. *Development* **145**.

Chan, S.W., Lim, C.J., Chong, Y.F., Pobbati, A.V., Huang, C. & Hong, W. (2011) Hippo pathway-independent restriction of TAZ and YAP by angiomotin. *J Biol Chem* **286**, 7018-7026.

Chatzeli, L., Gaete, M. & Tucker, A.S. (2017) Fgf10 and Sox9 are essential for the establishment of distal progenitor cells during mouse salivary gland development. *Development* **144**, 2294-2305.

Chen, Q., Zhang, N., Gray, R.S., Li, H., Ewald, A.J., Zahnow, C.A. & Pan, D. (2014) A temporal requirement for Hippo signaling in mammary gland differentiation, growth, and tumorigenesis. *Genes Dev* **28**, 432-437.

Delaleu, N., Jonsson, M.V., Appel, S. & Jonsson, R. (2008) New concepts in the pathogenesis of Sjogren's syndrome. *Rheum Dis Clin North Am* **34**, 833-845, vii.

Emmerson, E., May, A.J., Nathan, S., Cruz-Pacheco, N., Lizama, C.O., Maliskova, L., Zovein, A.C., Shen, Y., Muench, M.O. & Knox, S.M. (2017) SOX2 regulates acinar cell development in the salivary gland. *Elife* **6**.

Enger, T.B., Samad-Zadeh, A., Bouchie, M.P., Skarstein, K., Galtung, H.K., Mera, T., Walker, J., Menko, A.S., Varelas, X., Faustman, D.L., Jensen, J.L. & Kukuruzinska, M.A. (2013) The Hippo signaling pathway is required for salivary gland development and its dysregulation is associated with Sjogren's syndrome. *Lab Invest* **93**, 1203-1218.

Ewert, P., Aguilera, S., Alliende, C. *et al.* (2010) Disruption of tight junction structure in salivary glands from Sjogren's syndrome patients is linked to proinflammatory cytokine exposure. *Arthritis Rheum* **62**, 1280-1289.

Gao, T., Zhou, D., Yang, C., Singh, T., Penzo-Mendez, A., Maddipati, R., Tzatsos, A., Bardeesy, N., Avruch, J. & Stanger, B.Z. (2013) Hippo signaling regulates differentiation and maintenance in the exocrine pancreas. *Gastroenterology* **144**, 1543-1553, 1553 e1541.

George, N.M., Day, C.E., Boerner, B.P., Johnson, R.L. & Sarvetnick, N.E. (2012) Hippo signaling regulates pancreas development through inactivation of Yap. *Mol Cell Biol* **32**, 5116-5128.

Goto, H., Nishio, M., To, Y., Oishi, T., Miyachi, Y., Maehama, T., Nishina, H., Akiyama, H., Mak, T.W., Makii, Y., Saito, T., Yasoda, A., Tsumaki, N. & Suzuki, A. (2018) Loss of Mob1a/b in mice results in chondrodysplasia due to YAP1/TAZ-TEAD-dependent repression of SOX9. *Development* **145**.

Hai, B., Yang, Z., Millar, S.E., Choi, Y.S., Taketo, M.M., Nagy, A. & Liu, F. (2010) Wnt/beta-catenin signaling regulates postnatal development and regeneration of the salivary gland. *Stem Cells Dev* **19**, 1793-1801.

Hatzopoulos, S., Amoroso, C., Aimoni, C., Lo Monaco, A., Govoni, M. & Martini, A. (2002) Hearing loss evaluation of Sjogren's syndrome using distortion product otoacoustic emissions. *Acta Otolaryngol Suppl*, 20-25.

Hisatomi, Y., Okumura, K., Nakamura, K., Matsumoto, S., Satoh, A., Nagano, K., Yamamoto, T. & Endo, F. (2004) Flow cytometric isolation of endodermal progenitors from mouse salivary gland differentiate into hepatic and pancreatic lineages. *Hepatology*

**39**, 667-675.

Huang, C., Lu, H., Li, J., Xie, X., Fan, L., Wang, D., Tan, W., Wang, Y., Lin, Z. & Yao, T. (2018) SOX2 regulates radioresistance in cervical cancer via the hedgehog signaling pathway. *Gynecol Oncol* **151**, 533-541.

Hwang, S.M., Jin, M., Shin, Y.H., Ki Choi, S., Namkoong, E., Kim, M., Park, M.Y. & Park, K. (2014) Role of LPA and the Hippo pathway on apoptosis in salivary gland epithelial cells. *Exp Mol Med* **46**, e125.

Jonsson, R., Bolstad, A.I., Brokstad, K.A. & Brun, J.G. (2007) Sjogren's syndrome--a plethora of clinical and immunological phenotypes with a complex genetic background. *Ann N Y Acad Sci* **1108**, 433-447.

Kodama, S., Kuhtreiber, W., Fujimura, S., Dale, E.A. & Faustman, D.L. (2003) Islet regeneration during the reversal of autoimmune diabetes in NOD mice. *Science* **302**, 1223-1227.

Lee, M.J., Kim, E.J., Otsu, K., Harada, H. & Jung, H.S. (2016) Sox2 contributes to tooth development via Wnt signaling. *Cell Tissue Res* **365**, 77-84.

Li, J., Li, Z., Wu, Y., Wang, Y., Wang, D., Zhang, W., Yuan, H., Ye, J., Song, X., Yang, J., Jiang, H. & Cheng, J. (2019) The Hippo effector TAZ promotes cancer stemness by transcriptional activation of SOX2 in head neck squamous cell carcinoma. *Cell Death Dis* **10**, 603.

Lombaert, I.M., Abrams, S.R., Li, L., Eswarakumar, V.P., Sethi, A.J., Witt, R.L. & Hoffman, M.P. (2013) Combined KIT and FGFR2b signaling regulates epithelial progenitor expansion during organogenesis. *Stem Cell Reports* **1**, 604-619.

Lonyai, A., Kodama, S., Burger, D. & Faustman, D.L. (2008) Fetal Hox11 expression patterns predict defective target organs: a novel link between developmental biology and autoimmunity. *Immunol Cell Biol* **86**, 301-309.

Madisen, L., Zwingman, T.A., Sunkin, S.M., Oh, S.W., Zariwala, H.A., Gu, H., Ng, L.L., Palmiter, R.D., Hawrylycz, M.J., Jones, A.R., Lein, E.S. & Zeng, H. (2010) A robust and high-throughput Cre reporting and characterization system for the whole mouse brain. *Nat Neurosci* **13**, 133-140.

Maehama, T., Nishio, M., Otani, J., Mak, T.W. & Suzuki, A. (2020) The role of Hippo-YAP signaling in squamous cell carcinomas. *Cancer Sci*.

Mahoney, J.E., Mori, M., Szymaniak, A.D., Varelas, X. & Cardoso, W.V. (2014) The

hippo pathway effector Yap controls patterning and differentiation of airway epithelial progenitors. *Dev Cell* **30**, 137-150.

Maruyama, E.O., Aure, M.H., Xie, X., Myal, Y., Gan, L. & Ovitt, C.E. (2016) Cell-Specific Cre Strains For Genetic Manipulation in Salivary Glands. *PLoS One* **11**, e0146711.

Mese, H. & Matsuo, R. (2007) Salivary secretion, taste and hyposalivation. *J Oral Rehabil* **34**, 711-723.

Murakami, S., Shahbazian, D., Surana, R., Zhang, W., Chen, H., Graham, G.T., White, S.M., Weiner, L.M. & Yi, C. (2017) Yes-associated protein mediates immune reprogramming in pancreatic ductal adenocarcinoma. *Oncogene* **36**, 1232-1244.

Nakatani, K., Maehama, T., Nishio, M., Goto, H., Kato, W., Omori, H., Miyachi, Y., Togashi, H., Shimono, Y. & Suzuki, A. (2017) Targeting the Hippo signalling pathway for cancer treatment. *J Biochem* **161**, 237-244.

Nishio, M., Goto, H., Suzuki, M., Fujimoto, A., Mimori, K. & Suzuki, A. (2015) The Hippo Signaling Pathway: A Candidate New Drug Target for Malignant Tumors. In: *Innovative Medicine: Basic Research and Development* (eds. K. Nakao, N. Minato & S. Uemoto), pp. 79-94. Tokyo.

Nishio, M., Hamada, K., Kawahara, K. *et al.* (2012) Cancer susceptibility and embryonic lethality in Mob1a/1b double-mutant mice. *J Clin Invest* **122**, 4505-4518.

Nishio, M., Maehama, T., Goto, H., Nakatani, K., Kato, W., Omori, H., Miyachi, Y., Togashi, H., Shimono, Y. & Suzuki, A. (2017) Hippo vs. Crab: tissue-specific functions of the mammalian Hippo pathway. *Genes Cells* **22**, 6-31.

Panciera, T., Azzolin, L., Fujimura, A., Di Biagio, D., Frasson, C., Bresolin, S., Soligo, S., Basso, G., Bicciato, S., Rosato, A., Cordenonsi, M. & Piccolo, S. (2016) Induction of Expandable Tissue-Specific Stem/Progenitor Cells through Transient Expression of YAP/TAZ. *Cell Stem Cell* **19**, 725-737.

Price, E.J. & Venables, P.J. (1995) The etiopathogenesis of Sjogren's syndrome. *Semin Arthritis Rheum* **25**, 117-133.

Reginensi, A., Scott, R.P., Gregorieff, A., Bagherie-Lachidan, M., Chung, C., Lim, D.S., Pawson, T., Wrana, J. & McNeill, H. (2013) Yap- and Cdc42-dependent nephrogenesis and morphogenesis during mouse kidney development. *PLoS Genet* **9**, e1003380.

Royce, L.S., Kibbey, M.C., Mertz, P., Kleinman, H.P., Baum, B.J. (1993) Human

neoplastic submandibular intercalated duct cells express an acinar phenotype when cultured on a basement membrane matrix. *Differentiation*. **52**, 247-255.

Saleh, J., Figueiredo, M.A., Cherubini, K. & Salum, F.G. (2015) Salivary hypofunction: an update on aetiology, diagnosis and therapeutics. *Arch Oral Biol* **60**, 242-255.

Schlegelmilch, K., Mohseni, M., Kirak, O., Pruszak, J., Rodriguez, J.R., Zhou, D., Kreger, B.T., Vasioukhin, V., Avruch, J., Brummelkamp, T.R. & Camargo, F.D. (2011) Yap1 acts downstream of alpha-catenin to control epidermal proliferation. *Cell* **144**, 782-795.

Schwartz-Arad, D., Arber, L., Arber, N., Zajicek, G. & Michaeli, Y. (1988) The rat parotid gland--a renewing cell population. *J Anat* **161**, 143-151.

Skouloudaki, K., Puetz, M., Simons, M. *et al.* (2009) Scribble participates in Hippo signaling and is required for normal zebrafish pronephros development. *Proc Natl Acad Sci U S A* **106**, 8579-8584.

Song, E.C., Min, S., Oyelakin, A., Smalley, K., Bard, J.E., Liao, L., Xu, J. & Romano, R.A. (2018) Genetic and scRNA-seq Analysis Reveals Distinct Cell Populations that Contribute to Salivary Gland Development and Maintenance. *Sci Rep* **8**, 14043.

Soyfoo, M.S., Steinfeld, S. & Delporte, C. (2007) Usefulness of mouse models to study the pathogenesis of Sjogren's syndrome. *Oral Dis* **13**, 366-375.

Sugiyama, Y., Sasajima, J., Mizukami, Y., Koizumi, K., Kawamoto, T., Ono, Y., Karasaki, H., Tanabe, H., Fujiya, M. & Kohgo, Y. (2016) Gli2 protein expression level is a feasible marker of ligand-dependent hedgehog activation in pancreatic neoplasms. *Pol J Pathol* **67**, 136-144.

Szymaniak, A.D., Mi, R., McCarthy, S.E., Gower, A.C., Reynolds, T.L., Mingueneau, M., Kukuruzinska, M. & Varelas, X. (2017) The Hippo pathway effector YAP is an essential regulator of ductal progenitor patterning in the mouse submandibular gland. *Elife* **6**.

Uka, R., Britschgi, C., Krattli, A., Matter, C., Mihic, D., Okoniewski, M.J., Gualandi, M., Stupp, R., Cinelli, P., Dummer, R., Levesque, M.P. & Shakhova, O. (2020) Temporal activation of WNT/beta-catenin signaling is sufficient to inhibit SOX10 expression and block melanoma growth. *Oncogene* **39**, 4132-4154.

van Noort, M., Meeldijk, J., van der Zee, R., Destree, O. & Clevers, H. (2002) Wnt signaling controls the phosphorylation status of beta-catenin. *J Biol Chem* **277**, 17901-

17905.

Velozo, J., Aguilera, S., Alliende, C., Ewert, P., Molina, C., Perez, P., Leyton, L., Quest, A., Brito, M., Gonzalez, S., Leyton, C., Hermoso, M., Romo, R. & Gonzalez, M.J. (2009) Severe alterations in expression and localisation of {alpha}6{beta}4 integrin in salivary gland acini from patients with Sjogren syndrome. *Ann Rheum Dis* **68**, 991-996.

Ventura, A., Kirsch, D.G., McLaughlin, M.E., Tuveson, D.A., Grimm, J., Lintault, L., Newman, J., Reczek, E.E., Weissleder, R. & Jacks, T. (2007) Restoration of p53 function leads to tumour regression in vivo. *Nature* **445**, 661-665.

Wang, G., Lu, X., Dey, P. *et al.* (2016) Targeting YAP-Dependent MDSC Infiltration Impairs Tumor Progression. *Cancer Discov* **6**, 80-95.

Wang, W., Huang, J., Wang, X., Yuan, J., Li, X., Feng, L., Park, J.I. & Chen, J. (2012) PTPN14 is required for the density-dependent control of YAP1. *Genes Dev* **26**, 1959-1971.

Ye, X., Wu, F., Wu, C., Wang, P., Jung, K., Gopal, K., Ma, Y., Li, L. & Lai, R. (2014) beta-Catenin, a Sox2 binding partner, regulates the DNA binding and transcriptional activity of Sox2 in breast cancer cells. *Cell Signal* **26**, 492-501.

Yin, H., Qin, C., Zhao, Y., Du, Y., Sheng, Z., Wang, Q., Song, Q., Chen, L., Liu, C. & Xu, T. (2017) SOX10 is over-expressed in bladder cancer and contributes to the malignant bladder cancer cell behaviors. *Clin Transl Oncol* **19**, 1035-1044.

Zhao, R., Fallon, T.R., Saladi, S.V., Pardo-Saganta, A., Villoria, J., Mou, H., Vinarsky, V., Gonzalez-Celeiro, M., Nunna, N., Hariri, L.P., Camargo, F., Ellisen, L.W. & Rajagopal, J. (2014) Yap tunes airway epithelial size and architecture by regulating the identity, maintenance, and self-renewal of stem cells. *Dev Cell* **30**, 151-165.

***Figure Legends***

***FIGURE 1. Mob1a/1b deletion in mouse SMG epithelium results in significant acinar cell hypoplasia and immature ductal cell hyperplasia.***

**(a)** Left: Representative macroscopic views of SMGs of 8–9-week old control and *ad*MOB1DKO mice 3 weeks after starting TAM treatment for 5 days (post-TAM). Scale bar, 0.5 cm. Middle: Quantitation of SMG weight at the indicated days post-TAM (n=3-7/group). Right: Total cell number of each SMG at 21 days post-TAM (n=7/group) was determined by counting cells after digestion with collagenase, hyaluronidase, and dispase as described in "Experimental Procedures." For all Figures, data are the mean ± SEM. $^{**}P<0.01$; $^{*}P<0.05$. **(b)** Upper left: H&E-stained sections of control and *ad*MOB1DKO SMG at 21 days post-TAM. Scale bar, 10 μm. Upper middle and right: Representative immunohistochemical analyses of AQP5 (upper middle; green) or CK7 (upper right; red) expression in control and *ad*MOB1DKO SMGs at 21 days post-TAM (n=6/group). Nuclei were stained with DAPI (blue). Scale bars, 20 μm. Lower: Quantitation of percentages of $AQP5^+$ or $CK7^+$ cells (left, middle) or cell number (right) of control and *ad*MOB1DKO SMGs at 21 days post-TAM (n=7/group). The cell numbers were calculated from total cell number of each SMG multiplied by the percentage of $AQP5^+$ and $CK7^+$ cells, respectively. **(c)** Upper: Representative immunohistochemical staining to detect $CK14^-CK7^+$ mature ductal cells and $CK14^+CK7^+$ immature ductal cells in SMGs of control and *ad*MOB1DKO mice at 21 days post-TAM (n=6/group). Scale bar, 20 μm. Lower: Quantitation of total cell numbers of the immature (left) and mature (right) ductal cells in the SMGs in the upper panel. (d) H&E-stained sections of control and *ad*MOB1DKO SMGs at 21 days post-TAM showing dysplastic enlarged nuclei in the mutant tissue. Scale bar, 10 μm.

***FIGURE 2. adMOB1DKO mice show impaired saliva production, accumulating inflammatory cells, and fibrosis similar to Sjögren's syndrome.***

**(a)** Quantitation of the total amount of saliva secreted in 60 min by control and *ad*MOB1DKO mice subjected to Pilocarpine stimulation *in vivo* (n=4/group). **(b)** Representative sections of control and *ad*MOB1DKO SMGs at 14 days post-TAM that were stained with H&E, anti-CD45 antibody, or Sirius Red. Scale bars, 20 μm. Nuclei

were counterstained with hematoxylin (top panels), DAPI (middle panels), and iron hematoxylin (bottom panels). Blue arrowheads, inflammatory cells; yellow arrowheads, fibroblasts.

***FIGURE 3. MOB1 deficiency has no effect on the proliferation or apoptosis of acinar cells but ductal cells show increased turnover.***

**(a)** Representative immunohistochemical images (left) and quantitation (right) of $PCNA^+$ cells (green) among $CK7^+$ ductal cells (red), $AQP5^+$ acinar cells (red), or total cells in control and *ad*MOB1DKO SMGs at 21 days post-TAM (n=6/group). **(b)** Representative immunohistochemical images (left) and quantitation (right) of $TUNEL^+$ cells (red) among $CK7^+$ ductal cells (green), $AQP5^+$ acinar cells (green), or total cells in control and *ad*MOB1DKOSMGs at 21 days post-TAM (n=6/group). For (a) and (b), nuclei were stained with DAPI. Scale bars, 10 μm.

***FIGURE 4. MOB1-deficient immortalized clonal salivary epithelial cells show impaired acinar cell differentiation, and MOB1-deficient SMGs contain acinar/ductal bi-lineage progenitors.***

(a) Quantitation of the fold increase in the expression of the indicated acinar (Aqp5 and Amy1a) and ductal (Krt19 and Krt7) lineage markers as determined by qPCR in *im*MOB1DKO cells before (-) and after (+) culture in Matrigel for 7 days (n=4-5/group). mRNA expression data were normalized to *Gapdh*. **(b)** Quantitation of the fold increase in expression of the indicated acinar and ductal lineage markers as determined by qPCR in *im*MOB1DKO cells that were cultured for 10 days in Matrigel with (+) or without (-) TAM (n=4-5/group). mRNA expression data were normalized to *Gapdh*. *Mob1a* as inhibitory control after TAM. **(c)** Representative immunofluorescent detection (left) and quantification (right) of $AQP5^+CK14^+$ (double positive) immature ductal cells (white arrowhead) among total $CK14^+$ ductal cells in control and *ad*MOB1DKO SMGs at 21 days post-TAM (n=6/group). Scale bar, 10 μm.

***FIGURE 5. MOB1-mediated regulation of TAZ rather than YAP1 controls adult salivary epithelial cell homeostasis.***

**(a)** Immunoblot to detect total TAZ and YAP in total extracts of control and

*adMOB1*DKO SMGs at 21 days post-TAM. Actin, loading control. **(b)** Immunostaining to detect total TAZ and YAP1 in control and *adMOB1*DKO SMGs at 21 days post-TAM. Scale bar, 20 μm. For (a) and (b), data are representative of three independent experiments. **(c)** Left: Representative H&E-stained sections of SMGs from control, *ad*MOB1DKO, *ad*TAZTKO and *ad*YAPTKO mice at 21 days post TAM (n=5/group). White arrowheads, acinar cells. Scale bar, 20 μm. Right: Quantitation of the percentages of acinar cells among total cells of the SMGs in the left panel (n=5/group).

***FIGURE 6. MOB1-deficient salivary epithelial cells show inactivation of SOX2 and SOX10, but activation of β-catenin.***

**(a, b)** Representative immunostaining (left) and quantification of the intensities of nuclear SOX2, SOX10 **(a)** and active β-catenin (**b)**, in SMGs of control and *adMOB1*DKO mice at 21 days post-TAM (n=5/group). Represents are relative intensities of these molecules in *adMOB1*DKO mice to those of control mice. Scale bars, 20 μm.

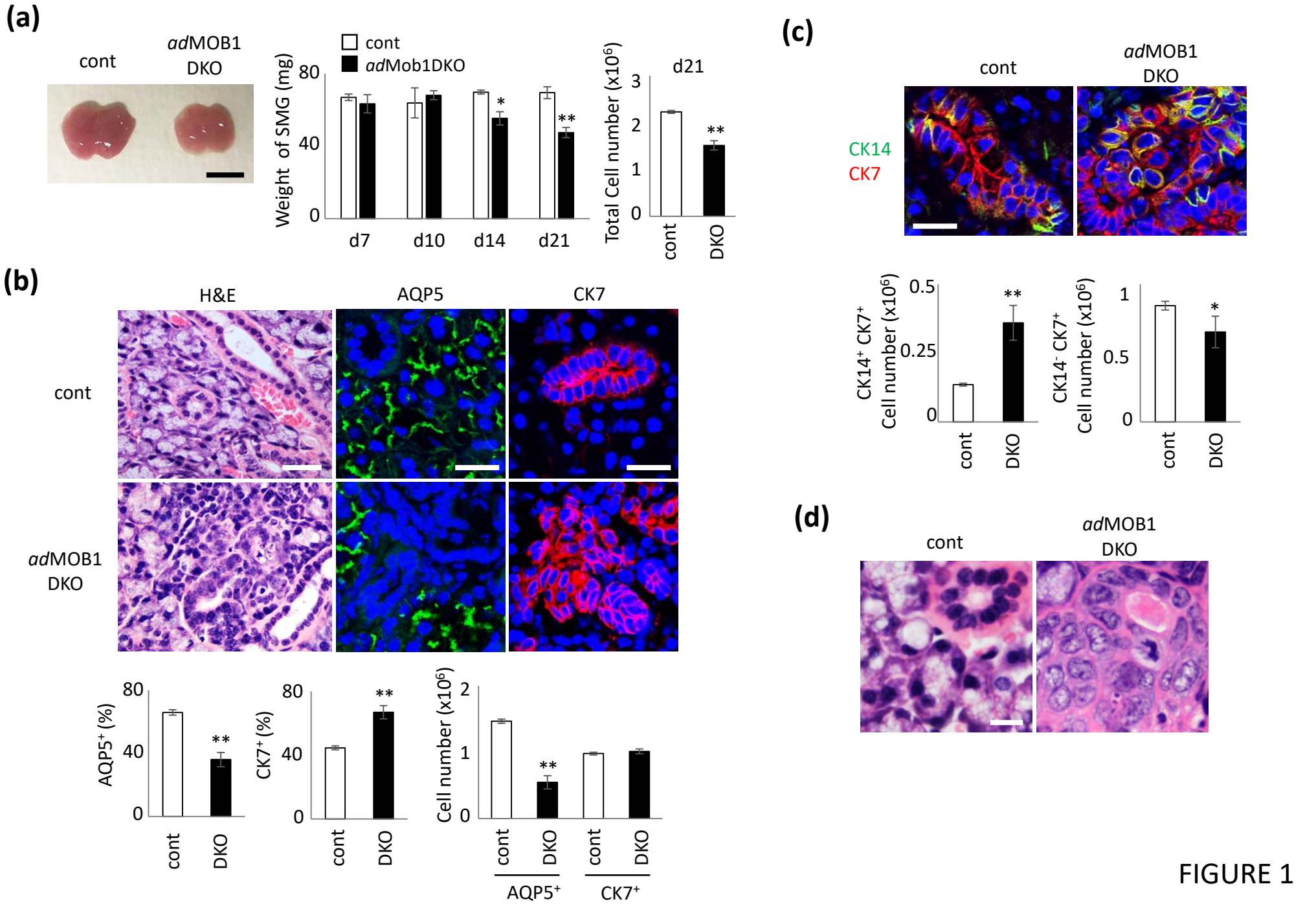
(a)
cont
adMOB1 DKO
cont
adMob1DKO
Weight of SMG (mg)
80
40
0
d7
d10
d14
d21
*
**
Total Cell number (x10⁶)
d21
3
2
1
0
**
cont
DKO
(b)
H&E
AQP5
CK7
cont
adMOB1 DKO
AQP5⁺ (%)
80
40
0
**
cont
DKO
CK7⁺ (%)
80
40
0
**
cont
DKO
Cell number (x10⁶)
2
1
0
**
cont
DKO
cont
DKO
AQP5⁺
CK7⁺
(c)
cont
adMOB1 DKO
CK14
CK7
CK14⁺ CK7⁺ Cell number (x10⁶)
0.5
0.25
0
**
cont
DKO
CK14⁻ CK7⁺ Cell number (x10⁶)
1
0.5
0
*
cont
DKO
(d)
cont
adMOB1 DKO

FIGURE 1

**(a)**

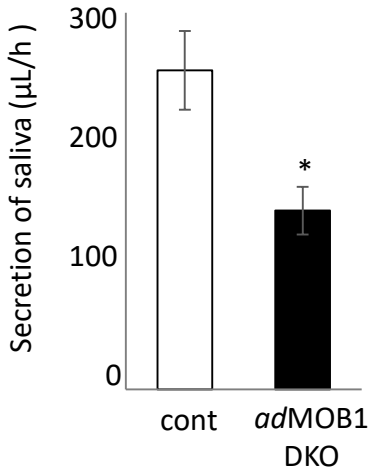
Secretion of saliva (μL/h )
300
200
100
0
*
cont
adMOB1
DKO

**(b)**

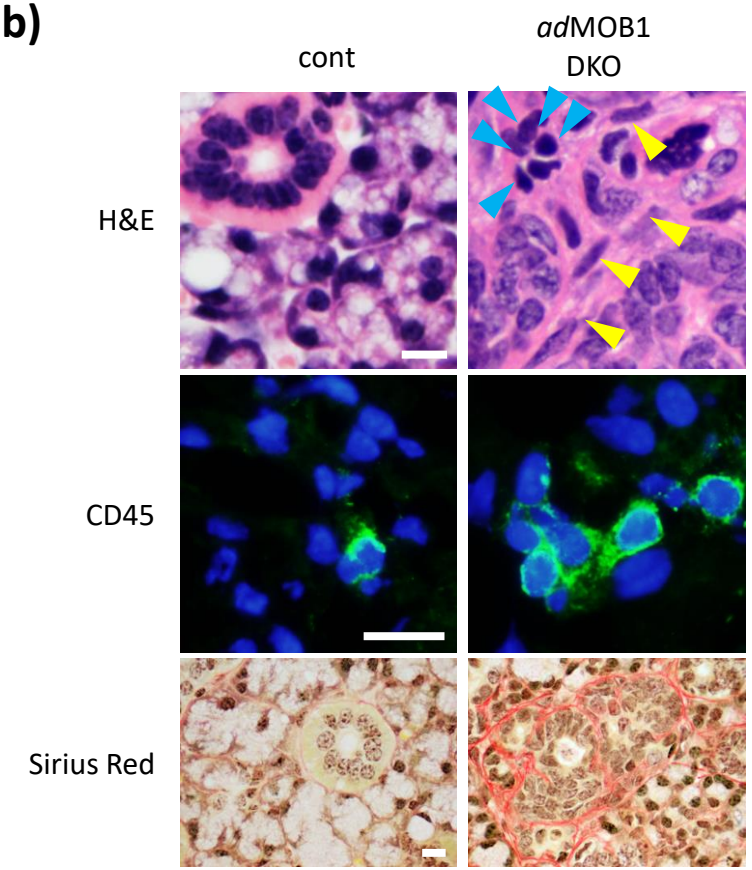
cont
adMOB1
DKO
H&E
CD45
Sirius Red

FIGURE 2

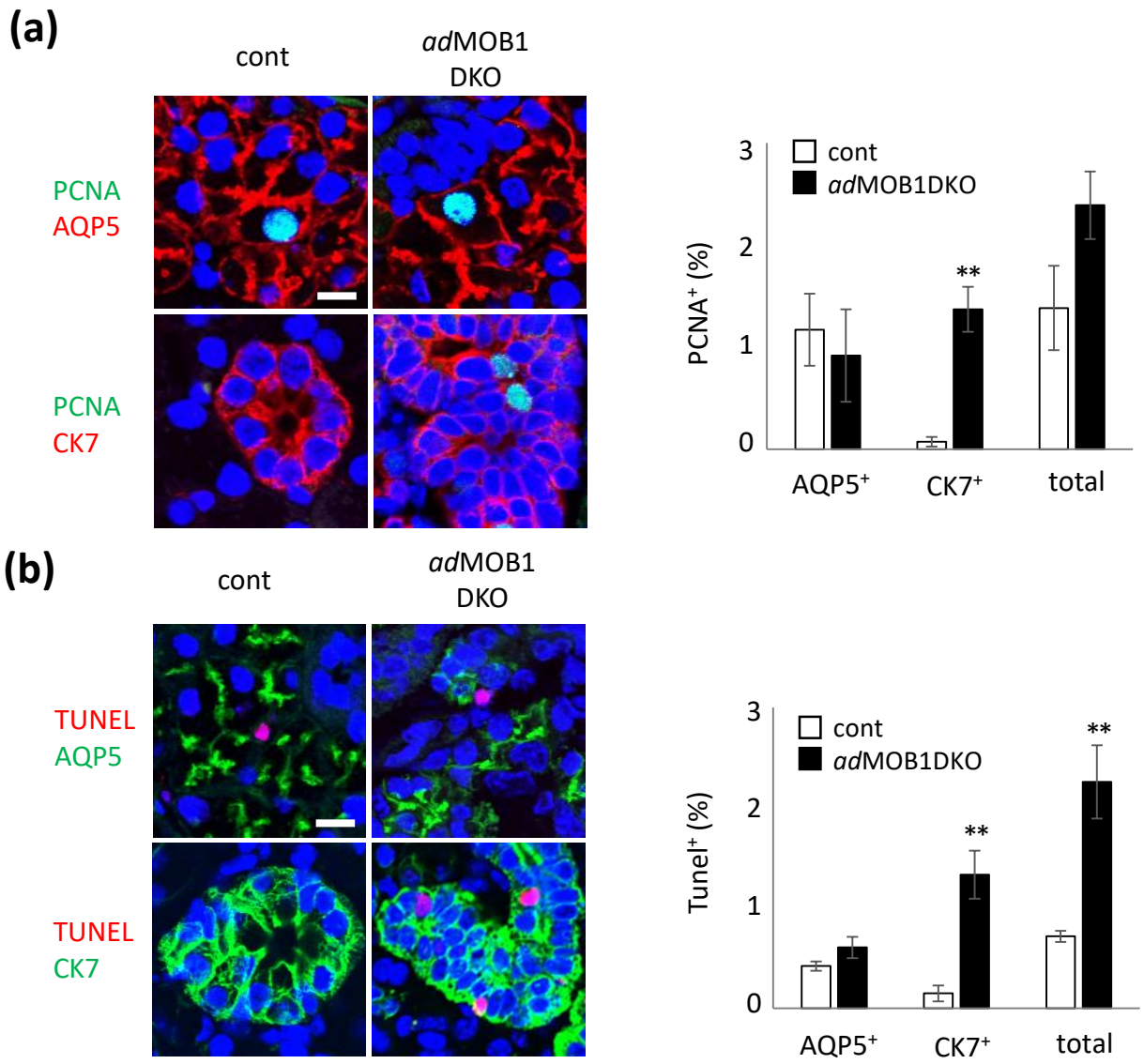
(a)
cont
adMOB1 DKO
PCNA
AQP5
PCNA
CK7
cont
adMOB1DKO
PCNA+ (%)
3
2
1
0
**
AQP5+
CK7+
total
(b)
cont
adMOB1 DKO
TUNEL
AQP5
TUNEL
CK7
cont
adMOB1DKO
Tunel+ (%)
3
2
1
0
**
**
AQP5+
CK7+
total

FIGURE 3

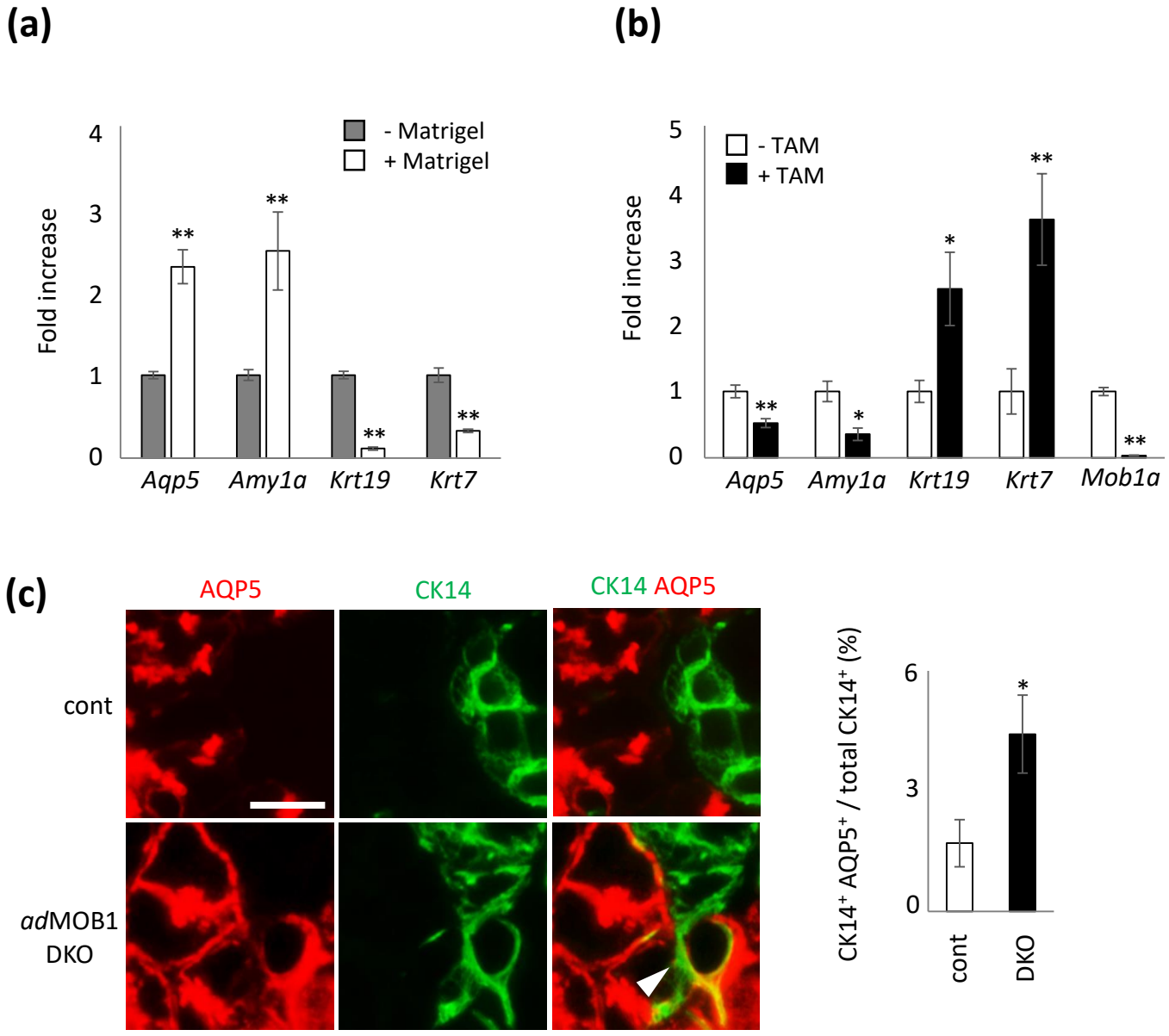
(a)
- Matrigel
+ Matrigel
Fold increase
Aqp5
Amy1a
Krt19
Krt7
(b)
- TAM
+ TAM
Fold increase
Aqp5
Amy1a
Krt19
Krt7
Mob1a
(c)
AQP5
CK14
CK14 AQP5
cont
adMOB1 DKO
CK14+ AQP5+ / total CK14+ (%)
cont
DKO

Figure 4

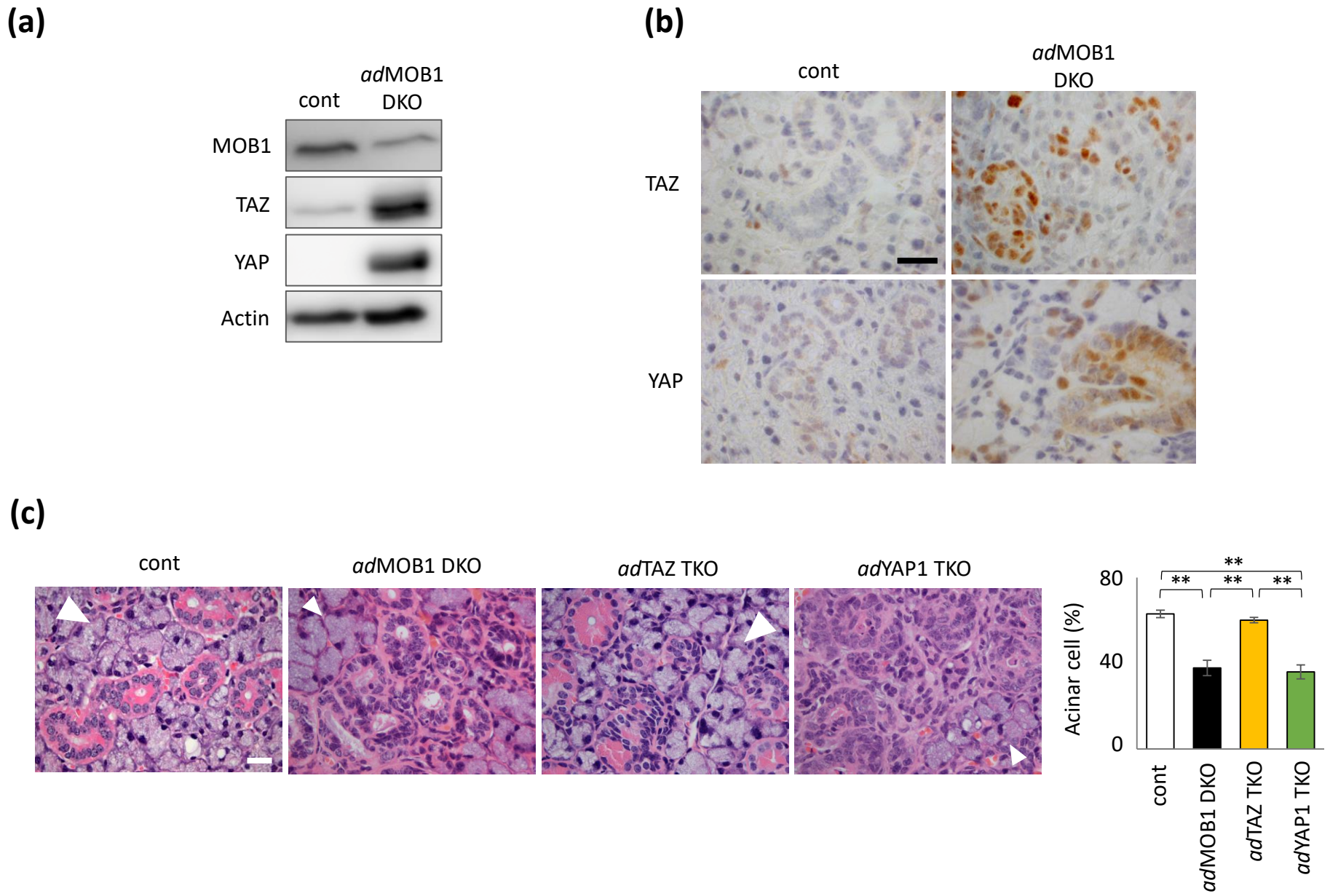
(a)
cont
adMOB1 DKO
MOB1
TAZ
YAP
Actin
(b)
cont
adMOB1 DKO
TAZ
YAP
(c)
cont
adMOB1 DKO
adTAZ TKO
adYAP1 TKO
Acinar cell (%)
80
40
0
**
**
**
**
cont
adMOB1 DKO
adTAZ TKO
adYAP1 TKO

FIGURE 5

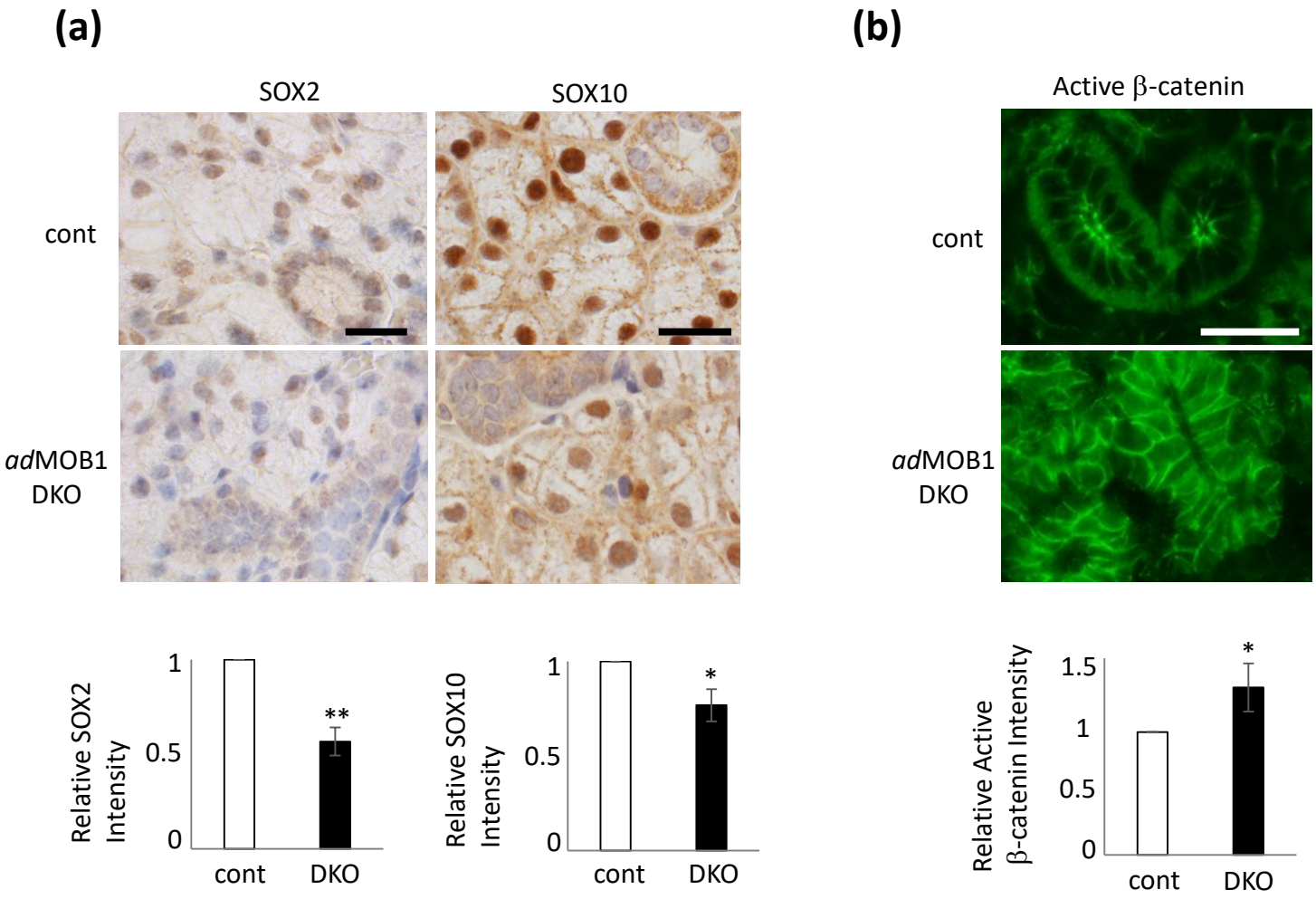
(a)
SOX2
SOX10
cont
adMOB1
DKO
Relative SOX2 Intensity
1
0.5
0
**
cont
DKO
Relative SOX10 Intensity
1
0.5
0
*
cont
DKO
(b)
Active β-catenin
cont
adMOB1
DKO
Relative Active β-catenin Intensity
1.5
1
0.5
0
*
cont
DKO

FIGURE 6

**Supplemental Information**

# TAZ inhibits acinar cell differentiation but promotes immature ductal cell proliferation in adult mouse salivary glands

Yosuke Miyachi[1,6], Miki Nishio[1,6], Junji Otani[1], Shinji Matsumoto[2], Akira Kikuchi[2], Tak Wah Mak[3,4,5], Tomohiko Maehama[1,7,8] and Akira Suzuki[1,7,8]

[1]Division of Molecular and Cellular Biology, Kobe University Graduate School of Medicine, Kobe, Japan

[2]Department of Molecular Biology and Biochemistry, Graduate School of Medicine, Osaka University, Suita, Japan

[3]The Princess Margaret Cancer Centre, University Health Network, Toronto, Canada

[4]Departments of Immunology and Medical Biophysics, University of Toronto, Toronto, Canada

[5]Department of Pathology, LKS Faculty of Medicine, The University of Hong Kong, Hong Kong, SAR

[6]Equal contribution as first author.

[7]Equal contribution as last author.

[8]Corresponding authors:

Tomohiko Maehama, Division of Molecular and Cellular Biology, Kobe University Graduate School of Medicine, Kusunoki-cho 7-5-1, Chuo-ku, Kobe, Hyogo, 650-0017, Japan
Tel:+81-78-382-6052; Fax:+81-78-382-6053; E-mail: tmaehama@med.kobe-u.ac.jp

Akira Suzuki, Division of Molecular and Cellular Biology, Kobe University Graduate School of Medicine, Kusunoki-cho 7-5-1, Chuo-ku, Kobe, Hyogo, 650-0017, Japan.
Tel:+81-78-382-6051; Fax:+81-78-382-6053; E-mail: suzuki@med.kobe-u.ac.jp

## Supplementary Table

***Table S1. List of primer sequences for genotyping and qPCR.***

| Gene | Forward Primer | Reverse Primer | Product Size (bp) |
|---|---|---|---|
| Primers for typing | | | |
| *Mob1a (wt allele)* | GTCTCGTGAAGGGTCTTGAGG | CCTGGTTGGGGTGGAGAATCAA | 319 (wt)<br>450 (flox) |
| *Mob1a (Δ allele)* | GTAATGTGTTCAGCTATGCTTTGAC | CCTGGTTGGGGTGGAGAATCAA | 551 |
| *Mob1b (wt allele)* | CTTCAGGATCCTTGGTGGTTATCAG | AGAGCAAGGGGAAAAGAAGCTCAATG | 586 |
| *Mob1b (Δ allele)* | CTTCAGGATCCTTGGTGGTTATCAG | TCAGGGTCACAAGGTTCATATGGTG | 673 |
| *Yap1* | GCCCAAACATACCCACGTAAT | CAGTCCAGTCAAGACAAGAT | 192 (wt)<br>336 (flox) |
| *Wwtr1 (Taz)* | AAGCAGTTTCCACTTCATGAAAC | AGTCAAGAGGGGCAAAGTTGTGA | 250 (wt)<br>330 (flox) |
| *Rosa26-CreERT2-Tg* | AAAGTCGCTCTGAGTTGTTAT | CCTGATCCTGGCAATTTCG | 825 |
| *Rosa26-LSL-tdTomato* | GGCATTAAAGCAGCGTATCC | CTGTTCCTGTACGGCATGG | 196 |
| Primers for qPCR | | | |
| *Amy1a* | CAGCACTTGTGGCAATGACTGG | GCAAAAGGCTGACCATTGACGAC | 96 |
| *Aqp5* | ATTGGCTTGTCGGTCACACT | GGAGGGGAAAAGCAAGTAGA | 192 |
| *Krt7 (CK7)* | AGGAGATCAACCGACGCAC | GTCTCGTGAAGGGTCTTGAGG | 148 |
| *Krt19 (CK19)* | GACCTAGCCAAGATCCTGAGT | TCAGCTCCTCAATCCGAGCA | 109 |
| *Mob1a* | GGCTAGCGAGGATGAGCTTC | CCTCAGATTGCCACTTCCGA | 137 |
| *Gapdh* | CACTGCCACCCAGAAGACTG | GTGAGCTTCCCGTTCAGCTC | 114 |

**Supplementary Figure Legends**

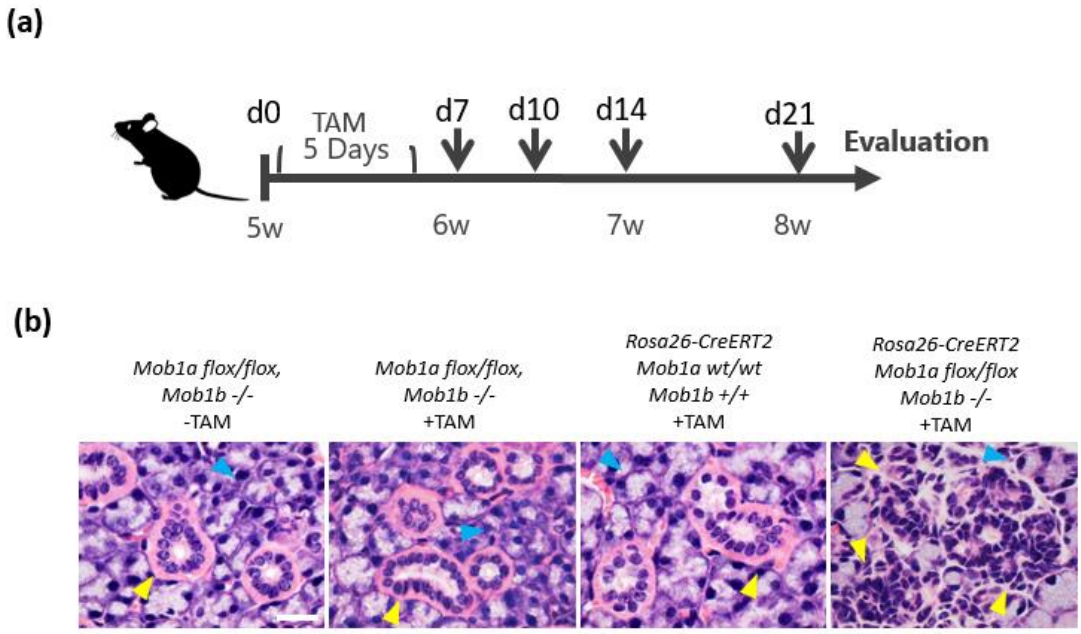


***Fig. S1. Protocol to generate postnatal Mob1a/1b DKO mice (adMOB1DKO) and their controls.***

**(a)** Diagram of the protocol used to generate *ad*MOB1DKO mice. *Mob1a*$^{flox/flox}$;*Mob1b*$^{-/-}$ mice were crossed to *Rosa26-CreERT2*-Tg mice to produce Rosa26-CreERT2;*Mob1a*$^{flox/flox}$;*Mob1b*$^{-/-}$ and control *Mob1a*$^{flox/flox}$;*Mob1b*$^{-/-}$ progeny. When the progeny were 35-42 days old, tamoxifen (TAM) was i.p. administered for 5 days. Mice were then sacrificed on the indicated days post-TAM initiation. **(b)** H&E-stained sections of SMGs from mice of the indicated genotypes at 3 weeks after starting TAM application (+TAM) or not (-TAM). Scale bar, 20 μm. Blue arrowheads, acinar cells; yellow arrowheads, ductal cells. Results shown are representative of at least three independent trials.

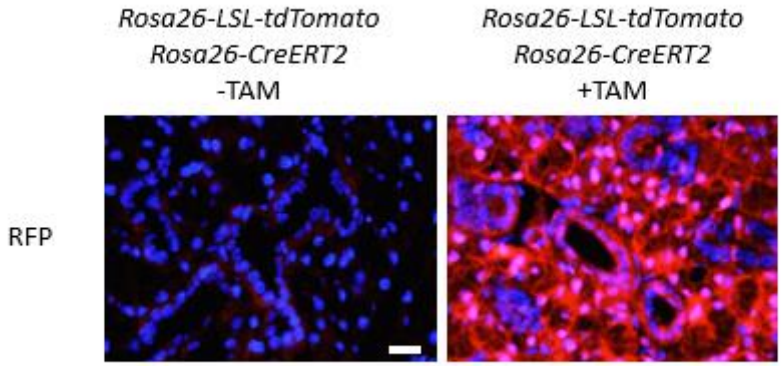


***Fig. S2. Confirmation of gene deletion in adMOB1DKO mice.***

Representative immunofluorescent staining to visualize target DNA (*Mob1a*) in SMGs of *Rosa26-CreERT2*; *Mob1a*$^{flox/flox}$;*Mob1b*$^{-/-}$ mice that expressed the *Rosa26-LSL-tdTomato* transgene and were treated with (+) or without (-) TAM i.p. for 5 days. Sections were stained with anti-RFP antibody to detect *tdTomato* expression. Scale bar, 20 μm. *Mob1a* deletion was observed in most of the cells in the mutant SMG.

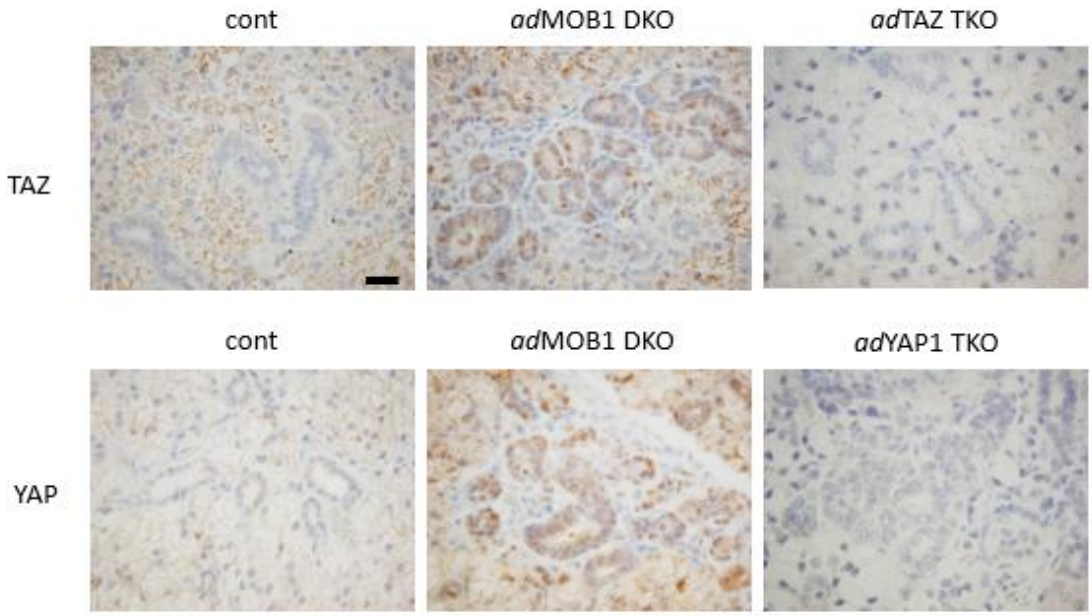


***Fig. S3. Confirmation of deletion of TAZ or YAP1 in triple knockout (TKO) MOB1A/1B-deficient mice.***

Representative immunohistochemical analyses to detect total TAZ or YAP1 in SMGs of control (left), *ad*MOB1DKO (middle), and MOB1A/1B & TAZ TKO (*ad*TAZ TKO; *Rosa26-CreERT2;Mob1a*$^{flox/flox}$*;Mob1b*$^{-/-}$*;Taz*$^{flox/flox}$*;*+TAM) (right, top); or MOB1A/1B & YAP TKO (*ad*YAP1 TKO*; Rosa26-CreERT2;Mob1a*$^{flox/flox}$*;Mob1b*$^{-/-}$*;Yap1*$^{flox/flox}$*;*+TAM) (right, bottom) mice. TAZ or YAP1 expression was deleted in most of the cells in SMGs of *ad*TAZ TKO or *ad*YAP1 TKO mice, respectively. Scale bar, 20 μm.

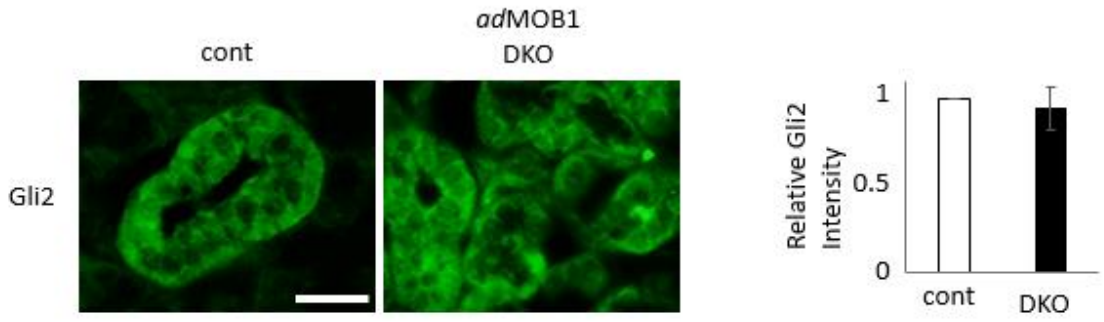


***Fig. S4. MOB1-deficiency did not alter GLI2 expression in salivary epithelial cells***

Representative immunostaining (left) and quantification of GLI2 **(a)** in SMGs of control and *adMOB1*DKO mice at 21 days post-TAM (n=5/group). Scale bars, 20 μm.

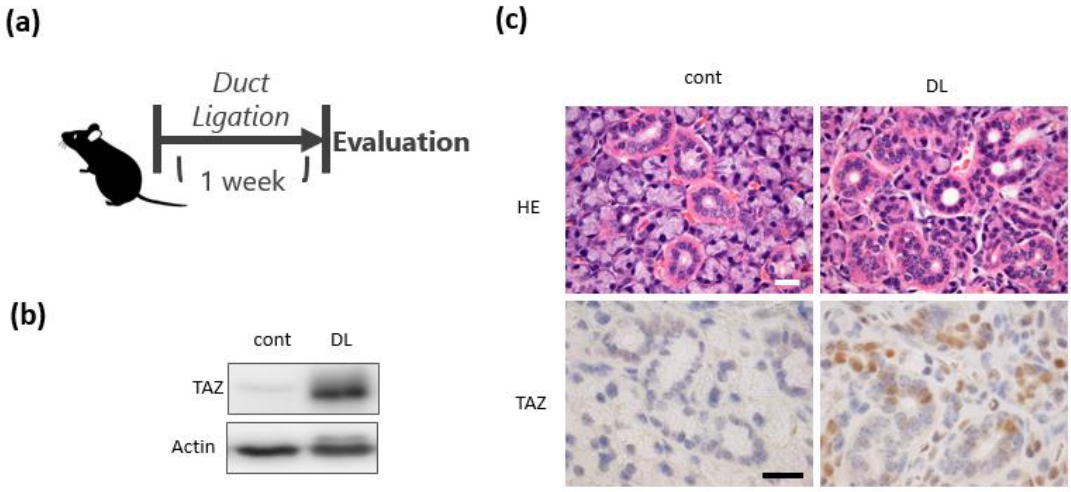


***Fig. S5. TAZ is activated by duct ligation.***

**(a)** Diagram of the protocol to achieve salivary duct ligation in mice. Control mice (5-week old) were subjected (or not) to duct ligation and sacrificed 1 week later. **(b)** Immunoblot to detect TAZ in SMGs of control (cont) and duct-ligation (DL) operated. Data are representative of three independent experiments. Actin, loading control. **(c)** H&E staining (upper) and immunostaining to detect TAZ (lower) in SMGs of the mice in (b). (n=3/group). Scale bars, 20 μm.